Delay-Based Macromodeling of Long Interconnects From Frequency-Domain Terminal Responses

Alessandro Chinea, Piero Triverio, *Student Member, IEEE*, and Stefano Grivet-Talocia, *Senior Member, IEEE*

***Abstract*—We present a robust and efficient scheme for the generation of delay-based macromodels from frequency-domain tabulated responses. These responses can come from both simulation or direct measurement. The main algorithm is based on an iterative weighted least-squares process for the identification of delayed rational approximations. In case that pole relocation is performed during the iterations, the scheme can be interpreted as a generalization of the well-known vector fitting algorithm to delayed systems. Therefore, we denote this algorithm as delayed vector fitting (DVF). In case no pole relocation is performed, the scheme generalizes the so-called Sanathanan–Koerner iteration, calling for the denomination of delayed Sanathanan–Koerner algorithm. These techniques produce compact macromodels that are readily synthesized in SPICE-compatible equivalent circuits including delayed sources or ideal transmission line elements. These macromodels outperform classical rational macromodels in terms of simulation time. Several examples illustrate the advantages of proposed methodology.**

***Index Terms*—Delay extraction, high-speed interconnects, macromodeling, rational approximations, scattering parameters, transmission lines.**

I. Introduction and Motivation

INTERCONNECTS may have a dramatic impact on the signal integrity of electronic systems. Therefore, a careful assessment of the nonideal behavior of interconnects must be performed at various scales, from chip to package, board, and system level. Numerical simulations are employed for this task, using suitable interconnect models. Since signal integrity system-level simulations are commonly performed using circuit solvers, also interconnect models need to be cast, via a suitable macromodeling process, in a form that is compatible with such simulation engines.

Several macromodeling techniques are available according to different classes of structures. Interconnects that are electrically small at the highest frequency of interest can be approximated by lumped blocks characterized by rational transfer functions. Examples can be connectors, via fields, or small packages. For these structures, the vector fitting (VF) algorithm, in its various implementations [2]–[10], is the standard macromodeling tool.

When the electrical size of the interconnect increases due to its physical length, the number of poles in the above rational approximation may grow very large. This leads to inefficient models in the simulation phase. Moreover, a pure rational approximation of a structure that is characterized by a significant propagation delay inevitably leads to a nonzero response before the time-of-flight has elapsed. This effect, which is intrinsic in the structure of the model, may be the source of serious accuracy degradation in system-level simulations [11]. The relevance of these issues grows with the interconnect length and the maximum operating frequency.

The above difficulties are easily overcome for interconnects that may be represented as transmission lines, governed by the telegraphers' equations. In such case, there exist several techniques that explicitly extract the propagation delays [12]–[18], leading to macromodels that structurally take into account the correct physics of signal transmission. Unfortunately, not all electrically long interconnects may be represented with pure transmission line models. Examples can be buses made of a chain of various blocks, as typically found in all systems for chip-to-chip, chip-to-memory or even larger scale links, or equivalently, interconnects including discontinuities along their path.

In this work, we extend standard purely rational macromodeling techniques to the case of electrically long interconnects. We consider a model structure that explicitly includes propagation delay terms, mixed with suitable rational coefficients [19]–[21]. The resulting delayed rational approximation is computed from raw tabulated frequency data using an iterative weighted linear least squares process. The basic implementation is denoted as delayed Sanathanan–Koerner (DSK) iteration, since it generalizes the standard Sanathanan–Koerner (SK) estimation scheme [1] to the new delayed macromodel structure. If a pole relocation step is included at each iteration, we obtain a scheme denoted as delayed vector fitting (DVF), which generalizes the well-known purely rational VF algorithm [2].

This paper builds on preliminary results of [21] and shares the same objectives of [20], where time-domain responses are used for the model identification. Here, we directly process frequency-domain data, including scattering parameters coming from direct measurement.

This paper is organized as follows. Section II introduces the model structure. Section III describes the main model identification algorithm. Section IV presents the SPICE netlist synthesis process. Finally, Section V applies the proposed scheme to several test cases and real application examples.

II. Macromodels With Delays

We consider an arbitrary electrically long interconnect with p input/output ports and represented by an unknown transfer function $\mathbf{H}(s)$. Our aim is to identify an approximation of $\mathbf{H}(s)$

Manuscript received July 18, 2008; revised October 27, 2008. First published April 07, 2009; current version published February 26, 2010. This work was partially supported by IBM. This work was recommended for publication by Associate Editor J. Tan upon evaluation of the reviewers comments.

The authors are with the Department of Electronics, Politecnico di Torino, 10129 Torino, Italy (e-mail: alessandro.chinea@polito.it; piero.triverio@polito.it; stefano.grivet@polito.it).

Color versions of one or more of the figures in this paper are available online at http://ieeexplore.ieee.org.

Digital Object Identifier 10.1109/TADVP.2008.2010525

from the sampled frequency response of the system, available from numerical simulation or direct measurement. Let us denote the available response samples as

$$\mathbf{H}_k \in \mathbb{C}^{p\times p} \tag{1}$$

and the available frequency points as

$$\omega = \omega_1, \ldots, \omega_{\bar{k}}. \tag{2}$$

Without loss of generality, we restrict our attention to a single element $H_{ij}(s)$ of the transfer function. Results will be then generalized to the most general multiport case by applying the proposed algorithm to each element of the transfer function independently, and then combining the results in a multiport model. In order to simplify the notation, we will drop the subscripts $_{ij}$.

We assume that the interconnect is structured as a chain of cascaded blocks [21]. Each of these basic elements can be a transmission-line structure, a lumped block, or another (simpler) electrically-long 3-D interconnect. For this class of structures, it can be shown (see Appendix) that each element of the transfer function can be written as

$$H(s) = \sum_m Q_m(s) e^{-sT_m} \tag{3}$$

where T_m represent the physical delays due to the propagation of the electromagnetic field inside the structure. These delays are properly defined in time domain, and measure the time taken by an electromagnetic wave to travel from one port to another port through the interconnect [39]. In addition, since the interconnect is not assumed to be homogeneous, but composed by several different blocks, these delays take also into account the multiple reflections a wave may experience inside the structure. The terms $Q_m(s)$ are instead suitable frequency-dependent coefficients representing other effects such as attenuation and dispersion.

The above consideration naturally leads to the macromodel structure that we adopt in this work. Essentially, two approximations are applied to (3). First, the number of delays is truncated to a (small) finite number $\bar{m}$. Second, a rational approximation is applied to each coefficient $Q_m(s)$ which, in general, is not a rational function. The resulting delayed rational model is further represented as

$$H(s) \simeq \sum_{m=1}^{\bar{m}} \frac{\sum_{n=0}^{\bar{n}} R_{mn}\phi_n(s)}{\sum_{n=0}^{\bar{n}} r_n \phi_n(s)} e^{-s\tau_m} \tag{4}$$

where $\phi_n(s)$ are partial fractions

$$\phi_n(s) = \begin{cases} 1, & \text{for } n = 0 \\ \frac{1}{s-a_n}, & \text{for } n = 1, \ldots, \bar{n} \end{cases} \tag{5}$$

associated to a prescribed set of "basis" poles a_n, and the delays

$$\tau_1, \ldots, \tau_{\bar{m}} \tag{6}$$

are approximations to the dominant delays in (3).

We remark that a delayed-rational form can also be obtained by replacing the partial fraction functions $\phi_n(s)$ in (5) with polynomials $\{1, s, s^2, \ldots\}$ or other systems of rational basis functions (such as orthogonal rational functions [6]). Polynomials are ruled out here due to possible ill-conditioning of the resulting model fitting equations. Among different sets of rational functions, the partial fractions basis (5) is adopted here due to its simple form and its excellent approximation and numerical stability properties. Partial fractions are indeed exploited in state-of-the-art fitting algorithms, such as vector fitting (VF) [2]. The basis poles a_n are chosen to optimize the numerical conditioning of the model identification process. For this purpose, we resort to the widely adopted solution proposed in [2], with initial poles being linearly distributed over the data bandwidth $[\omega_1, \omega_{\bar{k}}]$ and close to the imaginary axis.

III. Model Identification

A. Estimation of Propagation Delays

The first stage for the identification of a delayed macromodel (4) is the estimation of the dominant delay terms (6) from the raw data. For this task, we adopt the algorithm described in [21], based on the so-called Gabor transform [38]. In this work, we define the Gabor transform starting from frequency domain instead of the more standard time-domain representation, as

$$\mathcal{G}(\omega, \tau) = \int_{-\infty}^{+\infty} H(j\xi) W^*_{\omega,\tau}(\xi) d\xi. \tag{7}$$

The "basis" functions

$$W_{\omega,\tau}(\xi) = W(\xi - \omega) e^{-j\xi\tau} \tag{8}$$

are amplitude-modulated (parameter τ is proportional to the number of oscillations) and frequency-shifted (parameter ω is the center of the translation) versions of a normalized Gaussian window

$$W(\xi) = \pi^{-1/4} e^{-\xi^2/2}. \tag{9}$$

If $W(\xi)$ were taken to be identically one, the definition in (7) would become (up to a normalization constant) exactly the inverse Fourier transform of $H(j\xi)$, which is the system impulse response $h(\tau)$. Hence, the variable τ has the physical meaning of time or time-delay.

The Gaussian window $W(\xi)$ in (7) plays the role of a sharp bandpass filter. Therefore, $\mathcal{G}(\omega, \tau)$ can be regarded as the inverse Fourier transform of $H(j\xi)$, but retaining only those frequency components located in a frequency band centered around ω. For this reason, $\mathcal{G}(\omega, \tau)$ belongs to the class of the so-called time-frequency transforms, since it provides a localization of the various components of H both in frequency ω and time τ.

Local maxima $(\tilde{\omega}_m, \tilde{\tau}_m)$ of $|\mathcal{G}(\omega, \tau)|^2$ pinpoint the location in time (delay) and frequency of the dominant energy contributions of $H(j\omega)$. It turns out that typical interconnect responses are characterized by well-separated single-delay components, see Fig. 1 for a graphical illustration. Therefore, the time (delay) coordinates of the local maxima $\tilde{\tau}_m$ provide good estimates for the individual propagation delays in (4).

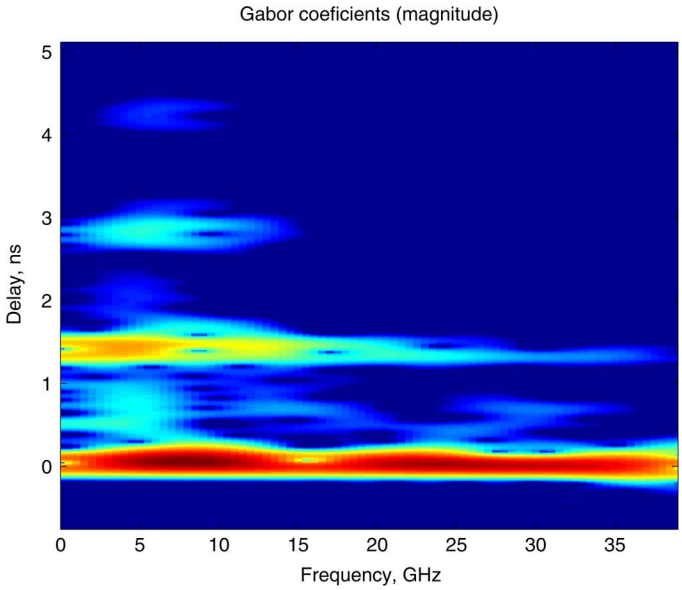

Fig. 1. Magnitude of Gabor coefficients for the return loss $S_{2,2}$ of a measured PCB interconnect. The same example will be analyzed in Section V-B.

The number of significant delays can be automatically determined as follows. First, we average the spectrogram $|\mathcal{G}(\omega,\tau)|^2$ over the available bandwidth Ω according to

$$\mathcal{G}_\omega^2(\tau) = \frac{1}{2\pi}\int_\Omega |\mathcal{G}(\omega,\tau)|^2 d\omega. \tag{10}$$

Then, starting from any local maximum $\tilde{\tau}_m$, we determine the closest local minimum $\tau_{\bar{m}}$ of $\mathcal{G}_\omega(\tau)$ such that $\tau_{\bar{m}} < \tilde{\tau}_m$. The energy content of the m-th individual delay term is thus estimated as

$$\mathcal{G}_m^2 = \frac{1}{2\pi}\int_{\tau_{\bar{m}}}^{\tau_{\bar{m}+1}} \mathcal{G}_\omega^2(\tau) d\tau. \tag{11}$$

All delay terms such that their relative contribution exceeds a predefined threshold γ

$$\frac{\mathcal{G}_m^2}{\sum_m \mathcal{G}_m^2} > \gamma \tag{12}$$

are retained in the model. Since the neglected energy contributions are small, this procedure does not significantly affect the accuracy of the final model. However, model efficiency is optimized, since the number of terms in (4) is minimal. More details on the actual implementation can be found in [21].

B. Model Coefficients Identification

Once the set of dominant delays (6) is known, the fundamental task is the estimation of the coefficients R_{mn} and r_n in (4), such that the deviation between model response and raw data is minimized at the available frequency points. We can define the approximation error at a single frequency point ω_k as

$$\mathcal{E}_k = H_k - \frac{\sum_{n=0}^{\bar{n}}\sum_{m=1}^{\bar{m}} R_{mn}\phi_n(j\omega_k)e^{-j\omega_k\tau_m}}{\sum_{n=0}^{\bar{n}} r_n\phi_n(j\omega_k)}. \tag{13}$$

The cumulative (rms) error for the entire response reads

$$\mathcal{E} = \sqrt{\frac{1}{\bar{k}}\sum_{k=1}^{\bar{k}} |\mathcal{E}_k|^2}. \tag{14}$$

It is clear that the cumulative error $\mathcal{E}$ is a complex nonlinear function of the unknown model coefficients R_{mn} and r_n. Main difficulty is the presence of the coefficients r_n at the denominator, which are responsible for the representation of the model poles.

This problem is solved by all modern strictly rational identification algorithms, such as VF, by an iterative weighting process known as SK iteration [1]. An outer iteration loop is devised. The ith pass of this loop minimizes a modified error metric obtained by multiplying (13) by a weighting factor

$$\mathcal{W}_k^{(i)} = \frac{\sum_{n=0}^{\bar{n}} r_n^{(i)}\phi_n(j\omega_k)}{\sum_{n=0}^{\bar{n}} r_n^{(i-1)}\phi_n(j\omega_k)} \tag{15}$$

which is the ratio between the (unknown) denominator at current iteration and the known denominator at previous iteration $i-1$. At the first iteration we set

$$r_n^{(0)} = \begin{cases} 1, & \text{for } n = 0 \\ 0, & \text{for } n = 1,\ldots,\bar{n} \end{cases} \tag{16}$$

as an initialization. The following single-frequency weighted error

$$\mathcal{E}_k^{(i)} = \frac{H_k\sum_n r_n^{(i)}\phi_n(j\omega_k) - \sum_n\sum_m R_{mn}^{(i)}\phi_n(j\omega_k)e^{-j\omega_k\tau_m}}{\sum_n r_n^{(i-1)}\phi_n(j\omega_k)} \tag{17}$$

is obtained. The above error is linear in the unknowns $R_{mn}^{(i)}$ and $r_n^{(i)}$, therefore its minimization is readily achieved by the solution of a standard linear least squares system, whose kth row is the right-hand side of (17). As an implementation detail, we add the following nontriviality constraint

$$\frac{1}{\bar{k}}\sum_k \mathbb{R}\mathrm{e}\left\{\frac{\sum_n\left(r_n^{(i)}-1\right)\phi_n(j\omega_k)}{\sum_n r_n^{(i-1)}\phi_n(j\omega_k)}\right\} = 0 \tag{18}$$

as a last row in the least squares system, in order to rule out the all-vanishing solution.

Iterations are stopped when all coefficients of the model representation are stabilized. Note that, upon convergence of the coefficients $r_n^{(i)}$, the weighting factor $\mathcal{W}_k^{(i)}$ tends to one uniformly, and the weighted least squares problem (17) becomes equivalent to the original formulation (13).

C. Stability Enforcement: DSK and DVF Schemes

Let us take a closer look at the rational approximation of a single-delay element

$$Q_m(s) \simeq \frac{R_{m0} + \sum_{n=1}^{\bar{n}} \frac{R_{mn}}{s-a_n}}{r_0 + \sum_{n=1}^{\bar{n}} \frac{r_n}{s-a_n}}. \tag{19}$$

Fundamental stability conditions require that the poles p_n of this rational function are constrained to the $\mathbb{R}\mathrm{e}\{s\} < 0$ region of the complex plane. This condition is readily checked by explicitly

computing the poles, i.e., zeros of the denominator, which are the eigenvalues of matrix

$$\begin{pmatrix} a_1-\rho_1 & -\rho_2 & \cdots & -\rho_{\bar{n}} \\ -\rho_1 & a_2-\rho_2 & \cdots & -\rho_{\bar{n}} \\ \vdots & \vdots & \ddots & \vdots \\ -\rho_1 & -\rho_2 & \cdots & a_{\bar{n}}-\rho_{\bar{n}} \end{pmatrix} \tag{20}$$

where $\rho_n = r_0^{-1} r_n$. In case of unstable poles, they are flipped into the left hand complex plane, and the corresponding new set of coefficients r_n in (19) is derived. This procedure forces the denominator to be a minimum phase rational function [2], [24], [33].

Two alternatives are possible for stepping through iterations. The first choice preserves the "basis" poles a_n through the iterations. The resulting scheme is a direct generalization of the SK iteration, which is therefore denoted as DSK (Delayed Sanathanan–Koerner) algorithm. The DSK scheme may be more robust, but unstable poles may appear at each iteration. The second choice updates also the "basis" poles a_n and, consequently, the partial fractions $\phi(s)$ of (5) at each iteration. This update is performed as follows. Starting from the poles $a_n^{(i-1)}$, the numerator of the weighting function (15) is formed as

$$\sigma(s) = r_0^{(i)} + \sum_{n=1}^{\bar{n}} \frac{r_n^{(i)}}{s - a_n^{(i-1)}}. \tag{21}$$

The zeros of this function define the set of poles $a_n^{(i)}$ to be used at next iteration. It is easily recognized that this scheme is a generalization of VF, which is thus denoted as delayed vector fitting (DVF). The DVF produces guaranteed stable models by construction, provided that the poles $a_n^{(i)}$ are constrained to the left hand plane by a suitable flipping process. Both DSK and DVF schemes will be applied to the various examples of Section V and compared.

D. Causality and Passivity

Passivity is a fundamental physical property [25], [26] which must be respected also by electrical models. For the class of structures under investigation, passivity conditions require both the causality of each response and the nonexpansivity (no energy gain) of the overall transfer matrix [27]. Causality conditions are satisfied by construction by the proposed algorithm, since each term in the model (3) is causal, because of the positivity of the delays T_m and the stability of the model poles [27]. If we assume that the raw data are passive, any possible passivity violation of the model will be small and of the same order of the approximation error that is achieved in the identification process. Therefore, passivity enforcement can be obtained using a perturbation approach, which is a standard practice for lumped macromodels [28]–[33]. Recent developments [34]–[37] extended such techniques to the class of delay-based macromodels, with specific attention to transmission-line macromodels based on the Method of Characteristics [36], [37]. Since the proposed model structure (3) falls in this class, it is argued that the perturbation approach of [36], [37] can be applied here after a suitable modification. These developments are outside the scope of this paper and will be documented in a future report.

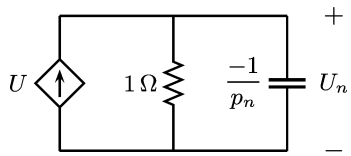

Fig. 2. Circuit synthesis of a single-pole partial fraction term.

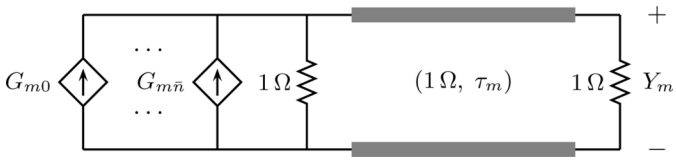

Fig. 3. Circuit synthesis of a single delay term in (23). The controlled sources are defined as $G_{mn} = K'_{mn} U_n$ for $n \neq 0$ and $G_{m0} = K_{m0} U$.

IV. Model Synthesis

In this section, we derive a compact SPICE-compatible circuit stamp for the delayed macromodel form (4). The first step is to rewrite the model expression as a summation of delayed partial fraction expansions

$$Y(s) = \sum_{m=1}^{\bar{m}} \left(K_{m0} + \sum_{n=1}^{\bar{n}} \frac{K_{mn}}{s - p_n} \right) e^{-s\tau_m} U(s) \tag{22}$$

where $U(s)$ and $Y(s)$ are the Laplace-domain input excitation and output response of the model. Due to the adopted model representation, the poles p_n are common to all delay terms. This allows us to decouple the synthesis of the rational part from the synthesis of the delays. In the following, we only provide details for real poles p_n, the case of complex poles being a trivial extension. We rewrite (22) as

$$Y(s) = \sum_{m=1}^{\bar{m}} \left(K_{m0} U(s) + \sum_{n=1}^{\bar{n}} K'_{mn} U_n(s) \right) e^{-s\tau_m} \tag{23}$$

with $K'_{mn} = -K_{mn} p_n^{-1}$ and where

$$U_n(s) = \frac{1}{1 - s/p_n} U(s) \tag{24}$$

represents the signal at the output of a one-pole lowpass filter, which can be synthesized by the single *RC* cell depicted in Fig. 2.

Depending on the adopted SPICE platform, the delay element can be synthesized in various ways. If delayed controlled sources are available, the synthesis of (23) is direct. If instead such elements are not available, delays can be synthesized using ideal transmission lines elements. We explore this second option in the following.

We need $\bar{m}$ different transmission line segments, since there are $\bar{m}$ distinct delays in (23). Application of a single delay τ_m is achieved by the circuit depicted in Fig. 3, representing a transmission line with unitary characteristic impedance, which is

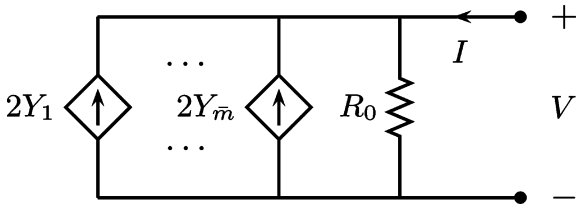

Fig. 4. Equivalent circuit connected at the model interface port. Scattering representation referred to R_0 port resistance is assumed.

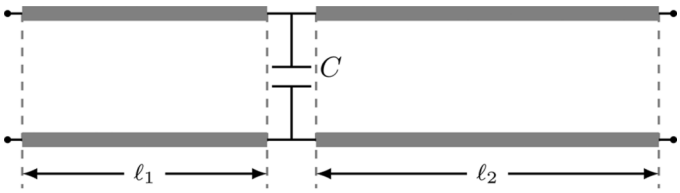

Fig. 5. Interconnect structure considered in Section V-A. Parameter values are $C = 1$ pF, $\ell_1 = 5$ m and $\ell_2 = 7$ m.

matched at both ends in order to avoid spurious signal reflections. The line is excited by a set of controlled sources which reproduce the summation over n in (23).

The outputs $Y_m(s)$ of the $\bar{m}$ delay lines are finally collected and reported to the output port via another set of controlled sources. The schematic of Fig. 4 represents the circuit that is directly connected to the output port, valid for scattering representations. In such case the model input is the impinging port wave, defined as $U(s) = R_0^{-1}V(s) + I(s)$, which feeds the single *RC* cells of Fig. 2. Since the matched ideal transmission line in Fig. 3 produces a current division factor equal to 0.5, the gain of the controlled sources in Fig. 4 is defined with a correction factor 2 to obtain a full equivalence to (23).

In case of multiport networks, the same synthesis process is performed for each pair of input–output couplings. This procedure is straightforward and not further commented here.

V. Examples

A. Synthetic Lumped-Distributed Network

This first example is intended to validate the delayed model identification approaches presented in Section III-B. We consider the structure depicted in Fig. 5, made of a chain of two transmission line segments with a capacitive discontinuity in between. The frequency-dependent per-unit-length parameters of the two transmission lines have been computed from dc up to 10 GHz using a surface-based method of moments (MoM) solver based on [23]. Conductor skin and proximity effects are explicitly taken into account. From this computation, we also obtain the asymptotic values of capacitance and inductance

$$C_\infty = 4.47 \times 10^{-11}\,\mathrm{F/m}, \quad L_\infty = 2.49 \times 10^{-7}\,\mathrm{H/m} \quad (25)$$

which are used to derive the nominal propagation delays of the two line segments

$$T_1 = \ell_1\sqrt{C_\infty L_\infty} = 1.67 \times 10^{-8}\,\mathrm{s}$$
$$T_2 = \ell_2\sqrt{C_\infty L_\infty} = 2.34 \times 10^{-8}\,\mathrm{s}. \quad (26)$$

TABLE I
Macromodeling Results for the Structure Depicted in Fig. 5

	Order			RMS Error $\times 10^{-3}$		
	VF	DSK	DVF	VF	DSK	DVF
$S_{1,1}$	1046	8	8	0.66	0.97	1.48
$S_{1,2}$	1124	8	8	0.77	0.58	0.58
$S_{2,2}$	1208	8	8	0.71	1.01	1.02

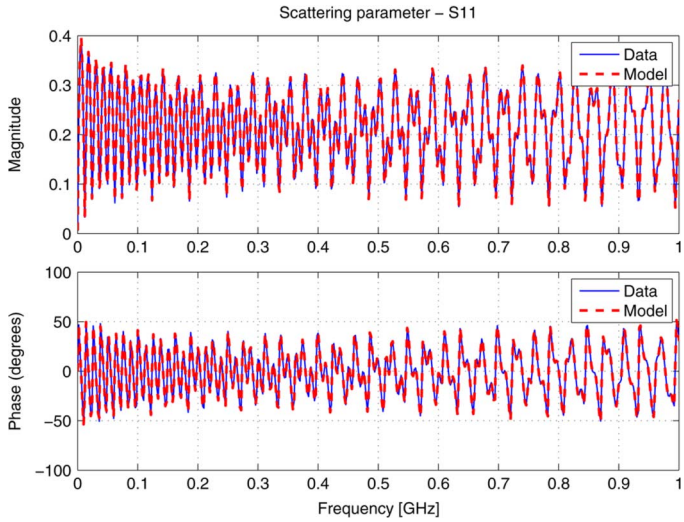

Fig. 6. Comparison between DVF model and data for the scattering element S_{11} of structure depicted in Fig. 5. Only a reduced bandwidth of 1 GHz is depicted in the figure for readability.

We can derive analytically the complete set of delays to be used in the macromodel expression

$$\tau^{1,1} = \tau^{2,2} = \left\{\sum_{i=1}^{2} 2m_iT_i : m_i \geq 0\right\}$$
$$\tau^{1,2} = \tau^{2,1} = \left\{\sum_{i=1}^{2} (2m_i+1)T_i : m_i > 0\right\} \quad (27)$$

where the superscripts indicate the respective scattering response. It is to be noted that, for $\tau^{1,1}$ not all the combinations of m_i are possible, in particular $m_2 > 0$ only if $m_1 > 0$. The same applies to $\tau^{2,2}$, for which $m_1 > 0$ only if $m_2 > 0$.

A total number $\bar{k} = 5001$ frequency samples with $\bar{m} = 6$ delay terms were used in the DSK and DVF model identification. We report in Table I the number of model poles used in the rational approximation, and the corresponding rms approximation errors obtained with the DSK and DVF algorithms. The table includes also the results of the standard VF scheme for comparison.

The approximation errors are well below engineering accuracy for all three algorithms. However, application of standard VF algorithm requires a very large number of poles for obtaining a purely rational approximation of the terminal scattering responses with a level of accuracy that is comparable with the DSK and DVF results. Conversely, due to the explicit extraction of the propagation delays, both DSK and DVF achieve excellent accuracy with a very small number of poles.

Figs. 6–8 compare the frequency-responses of the delayed macromodel to the raw data used for the model identification.

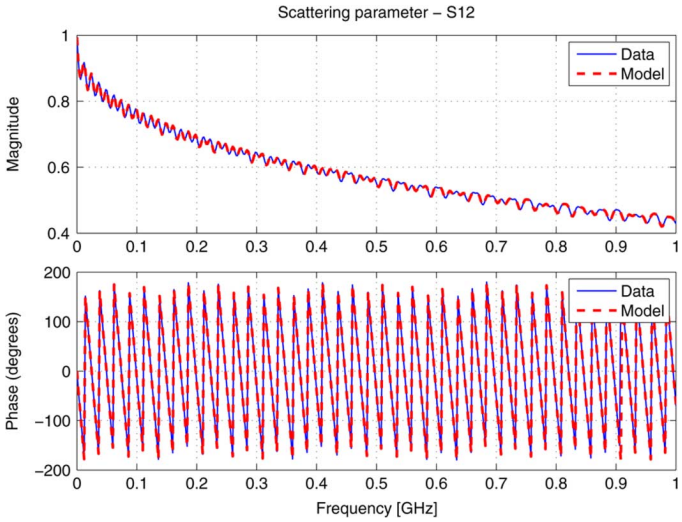

Fig. 7. As in Fig. 6, but for S_{12}.

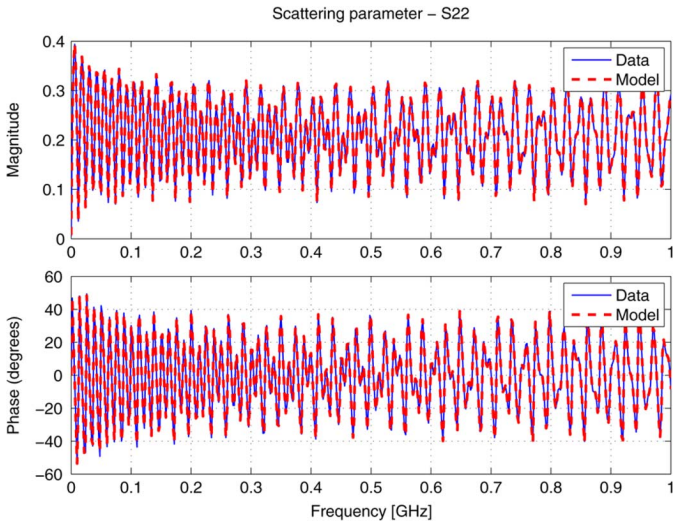

Fig. 8. As in Fig. 6, but for S_{22}.

We only report the results of DVF algorithm, since both VF and DSK results appear identical on this scale. Also, only one tenth of the modeling bandwidth is displayed for readability of the plots. Similar results are obtained over the full bandwidth up to 10 GHz. These statements are confirmed by Table I, which reports error metrics computed for all models over the entire bandwidth.

B. Measured PCB Interconnect

The second example is a 10-cm-long printed circuit board (PCB) interconnect. The structure, which includes signal launches and discontinuities, is characterized via measured scattering responses up to 40 GHz (courtesy of Prof. C. Schuster, formerly IBM). A total number of $\bar{k} = 801$ frequency samples are available. For this case, the delays are not known *a priori* and must be inferred from the data. The estimation procedure of Section III-A leads to the results of Table II. Fig. 1 reports an illustration of the time-frequency energy localization for $S_{2,2}$, which leads to the delay estimates reported in the table.

TABLE II
DELAYS ESTIMATES FOR THE PCB INTERCONNECT OF SECTION V-B

	τ_1	τ_2	τ_3	τ_4
$S_{1,1}$	0.00 ns	1.3 ns	2.64 ns	4.08 ns
$S_{1,2}$	0.66 ns	1.99 ns	3.37 ns	–
$S_{2,2}$	0.00 ns	1.3 ns	2.64 ns	4.08 ns

TABLE III
MACROMODELING RESULTS FOR THE PCB INTERCONNECT OF SECTION V-B

	Order			RMS Error $\times 10^{-2}$		
	VF	DSK	DVF	VF	DSK	DVF
$S_{1,1}$	72	16	16	0.91	1.38	1.38
$S_{1,2}$	72	16	16	0.64	0.63	0.63
$S_{2,2}$	76	16	16	0.92	1.00	1.19

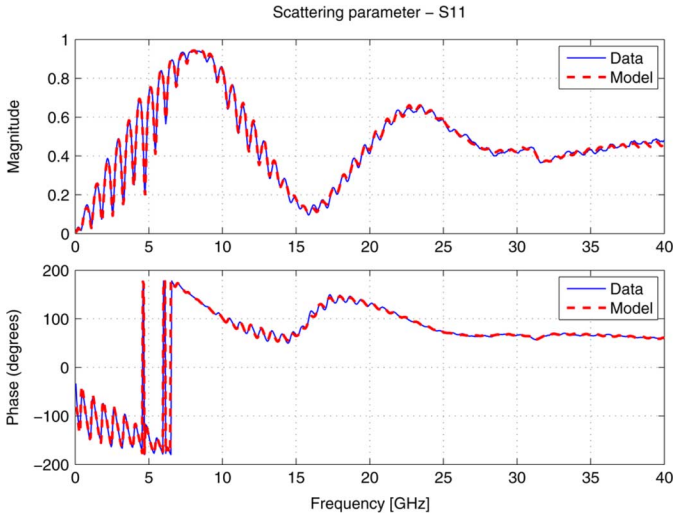

Fig. 9. Comparison between DVF model and data for the return loss S_{11} of the PCB interconnect of Section V-B.

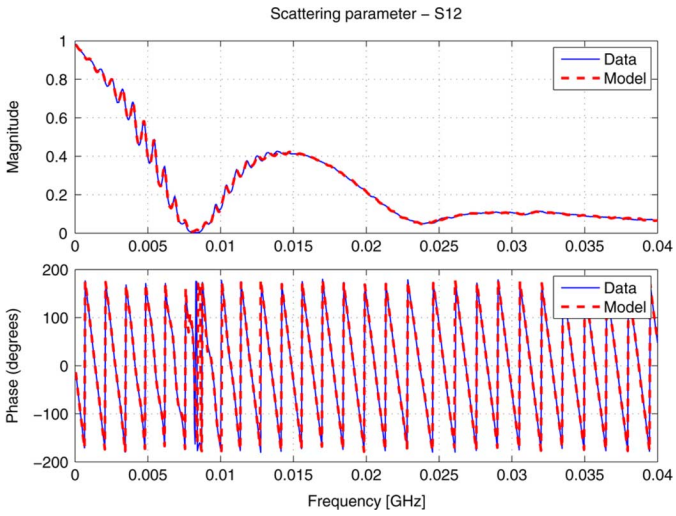

Fig. 10. As in Fig. 9, but for insertion loss S_{12}.

Table III reports the modeling parameters and results of the VF, DSK, and DVF algorithms. The level of approximation is excellent, taking into account that modeling accuracy cannot be as low as desired due to the measurement noise floor. Figs. 9–11 compare the DVF model responses to the corresponding raw

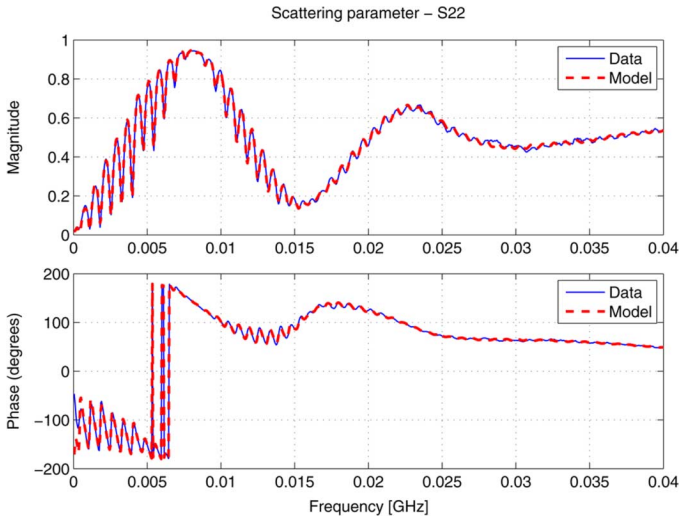

Fig. 11. As in Fig. 9, but for S_{22}.

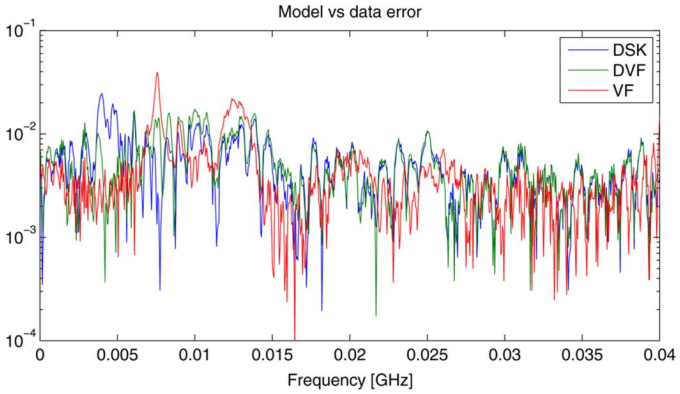

Fig. 12. Model vs data deviation for the scattering element S_{12} of the PCB interconnect of Section V-B.

TABLE IV
DELAYS ESTIMATES FOR THE COMPLEX BUS OF SECTION V-C

	τ_1	τ_2	τ_3	τ_4
$S_{1,1}$	0.00 ns	0.56 ns	5.44 ns	6.71 ns
$S_{2,2}$	0.00 ns	1.29 ns	5.87 ns	–
$S_{1,2}$	2.73 ns	–	–	–

TABLE V
MACROMODELING RESULTS FOR THE COMPLEX BUS OF SECTION V-C

	Order			RMS Error $\times 10^{-3}$		
	VF	DSK	DVF	VF	DSK	DVF
$S_{1,1}$	80	20	20	2.63	2.73	2.78
$S_{1,2}$	48	15	15	4.95	7.73	6.13
$S_{2,2}$	66	25	25	5.26	5.42	5.34

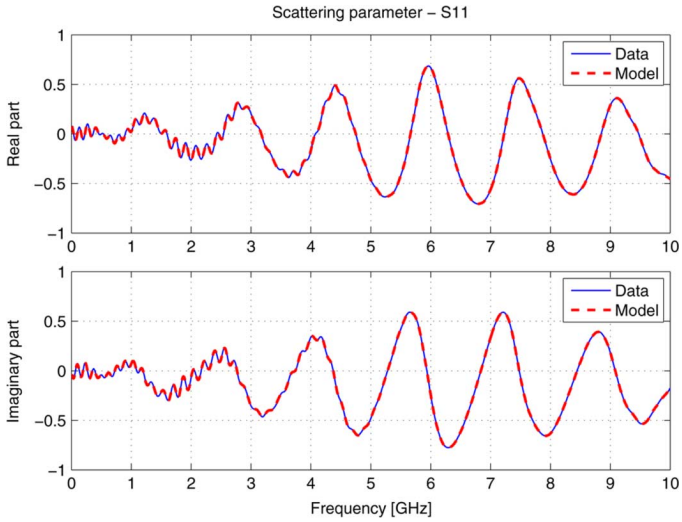

Fig. 13. Comparison between model and data for the return loss S_{11} of the complex bus of Section V-C.

measured data. Also for this case, no visible difference is evident from the plots. This applies also to the DSK and VF results, not reported. A confirmation is provided by Fig. 12, which reports the frequency-dependent model versus data error obtained by all three algorithms for the $S_{1,2}$ response.

C. Complex Bus

We now consider a complex bus structure, namely the IBM GX bus. The raw specification is a set of frequency-dependent scattering parameters (courtesy of IBM), obtained by cascading several different simpler models of lumped blocks and frequency-dependent transmission lines, and performing a simple frequency-domain solution of the interconnected system. Main task is to compute a global model from the terminal responses of the entire bus, without using any information on the internal structure.

For this structure, the number of dominant delays varies depending on the considered response. Table IV summarizes the various delays estimates that are used to extract the model.

Both delayed macromodeling schemes DSK and DVF and the classical strictly rational VF were applied, in order to compare model accuracy and complexity. The model identification results are summarized in Table V for the modeled scattering responses. The results show that a significant saving in terms of number of poles is achieved by DSK and DVF with respect to standard VF. The DSK produces a model that is not stable due to the presence of poles with positive real part. Conversely, the DVF model is stable and thus represents the best compromise between model accuracy and complexity.

Figs. 13–15 report a comparison between the global DVF model and the raw data, showing excellent correlation. Fig. 16 reports the magnitude of the S_{11} model versus data errors, which are uniformly bounded over frequency for all VF, DSK, and DVF algorithms.

D. Transient Analysis

We consider the three interconnect structures discussed in Sections V-A–V-C and we compare the performance in terms of accuracy and simulation time of the SPICE netlists corresponding to the VF and DVF macromodels. In all cases, we adopt the same model termination scheme, in order to draw meaningful conclusions. In particular, all model ports are matched into their reference resistance $R_0 = 50\,\Omega$. Each model is excited at one port using a single pulse, and the received voltage is monitored at the other interconnect port.

The results of the SPICE transient simulations are reported in the various panels of Fig. 17. We also include in Fig. 17(c) an additional structure, which is the same PCB interconnect of

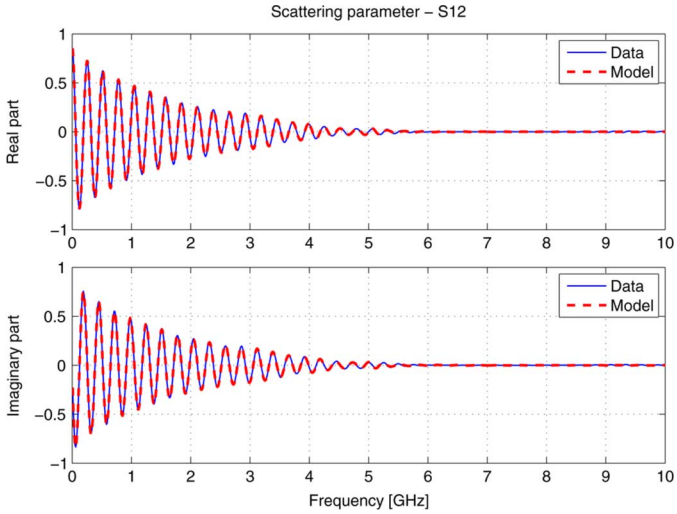

Fig. 14. As in Fig. 13, but for insertion loss S_{12}.

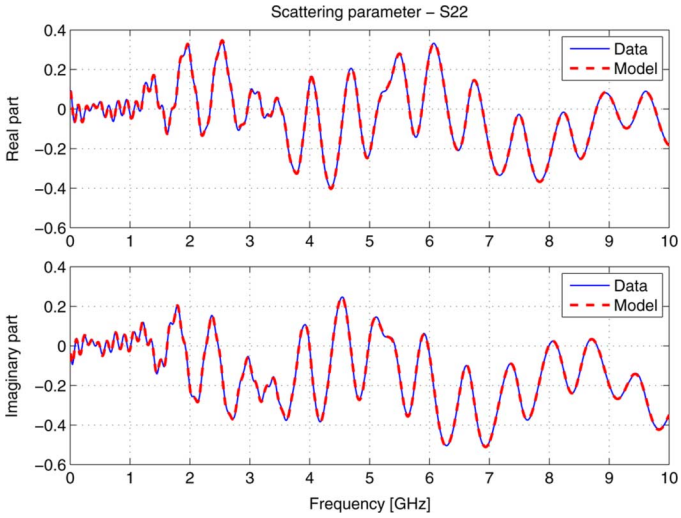

Fig. 15. As in Fig. 13, but for return loss S_{22}.

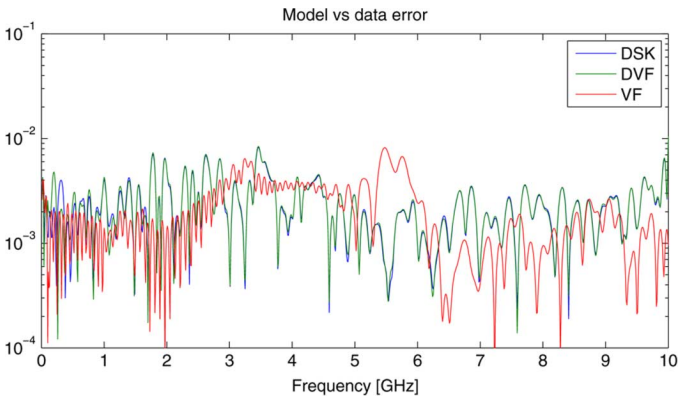

Fig. 16. Model versus data deviation for the scattering element S_{11} of the complex bus of Section V-C.

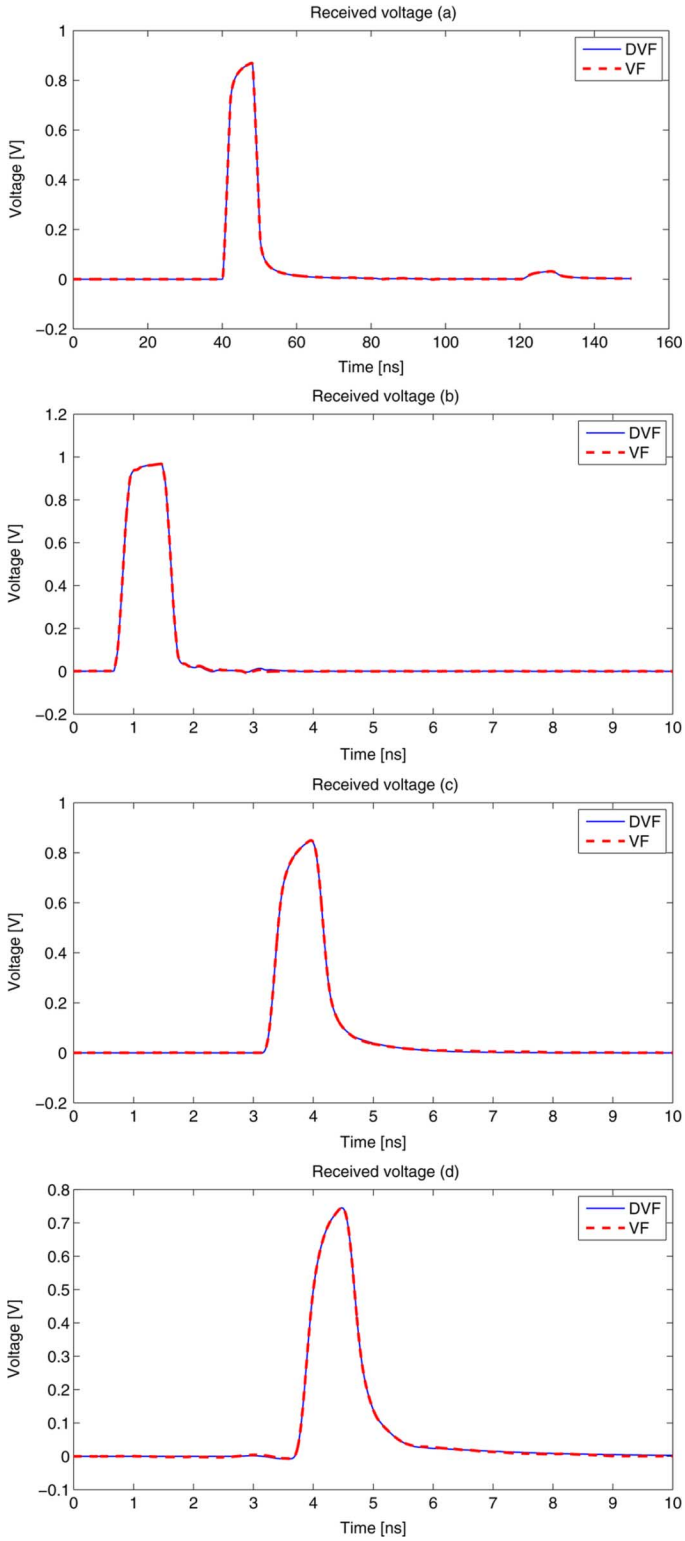

Fig. 17. Transient SPICE results for: (a) the distributed circuit of Section V.A; (b) the measured PCB interconnect of Section V.B; (c) as in (b), but with an interconnect length of 50 cm; (d) the bus structure of Section V.C.

Section V-B, but with a length of 50 cm. This structure is included with the aim of relating the macromodeling efficiency with the electrical length of the interconnect. In all cases, a quite good match is observed between the VF and DVF model.

However, a closer look at the results reveals that VF models produce spurious oscillations before the expected propagation delay has elapsed, since this delay is only approximated by VF via a finite-order rational function. Fig. 18 illustrates this for the 50-cm-long PCB interconnect. Conversely, the DVF models are

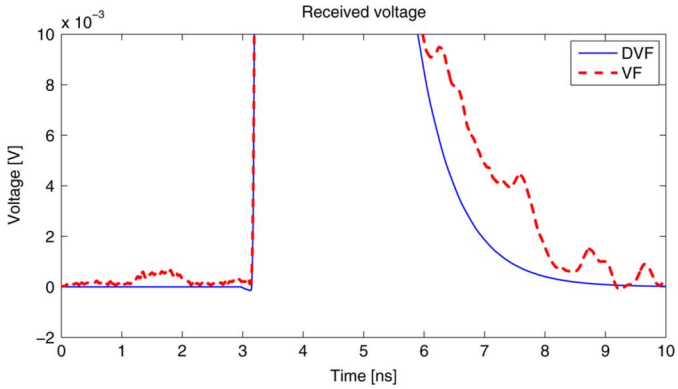

Fig. 18. Zoom of Fig. 17(c).

TABLE VI
TRANSIENT SPICE SIMULATION TIME

Structure	VF	DVF	Speedup
Sec. V-A	113 s	4.47 s	25X
Sec. V-B (10 cm)	2.77 s	1.30 s	2.1X
Sec. V-B (50 cm)	7.49 s	0.81 s	9.3X
Sec. V-C	1.84 s	0.80 s	2.3X

exempt from this inconsistency, since the delays are explicitly extracted and accounted for in the model.

We conclude by presenting in Table VI a summary of the CPU time required for the various transient simulations. It can be observed that the speedup factor of DVF with respect to standard VF macromodels scales almost linearly with the electrical size of the interconnect at the highest frequency of interest.

VI. CONCLUSION

We presented a new model identification algorithm for long interconnect links. The modeling strategy is based on a combination of propagation delay extraction and rational approximation in the frequency domain. The explicit inclusion of delay terms allows for a direct representation of rapid phase variations, whereas slowly varying variations are captured by low-order rational coefficients. Model identification is performed directly on terminal scattering responses via iterative solution of suitably weighted linear least-squares problems. This process leads to particularly compact models that can be readily synthesized into SPICE-compatible netlists, allowing for significant reduction of simulation times with respect to more standard purely rational macromodeling techniques.

APPENDIX

We prove in this Appendix that composite structures obtained by cascading lumped multiport elements and transmission line segments may be represented as in (3). We denote with $\mathcal{R}$ the set of the pseudorational transfer functions in the form

$$H(s) = \sum_m Q_m(s) e^{-sT_m} \tag{28}$$

where $Q_m(s)$ are proper rational transfer functions and the summation may include infinite terms. Also, we denote with $\mathcal{R}^{n\times k}$ the matrices $n \times k$ with the entries in $\mathcal{R}$. The proof is conducted for $k = n = 2$, since the generalization to larger port counts follows the same scheme.

We first prove that the cascade connection of two scattering matrixes $\mathbf{S}'(s) \in \mathcal{R}^{2\times 2}$ and $\mathbf{S}''(s) \in \mathcal{R}^{2\times 2}$ leads to a scattering matrix $\mathbf{S}(s)$ that also belongs to $\mathcal{R}^{2\times 2}$. Simple calculations show that connection of port 2 of $\mathbf{S}'(s)$ with port 1 of $\mathbf{S}''(s)$ leads to the following expressions:

$$\begin{aligned}
S_{11} &= S'_{11} + S'_{12}S''_{11}(1 - S'_{22}S''_{11})^{-1}S'_{21} \\
S_{12} &= S'_{12}(1 - S''_{11}S'_{22})^{-1}S''_{12} \\
S_{21} &= S''_{21}(1 - S'_{22}S''_{11})^{-1}S'_{21} \\
S_{22} &= S''_{22} + S''_{21}(1 - S'_{22}S''_{11})^{-1}S'_{22}S''_{12}.
\end{aligned} \tag{29}$$

Clearly, the set $\mathcal{R}$ is closed under the sum and product operations. Using the result

$$(1 - A)^{-1} = \sum_{m=0}^{\infty} A^m$$

valid for $|A| < 1$, we can conclude that $A \in \mathcal{R}$ implies $(1 - A)^{-1} \in \mathcal{R}$. Therefore, all elements of $\mathbf{S}(s)$ in (29) belong to $\mathcal{R}$. The above result can be applied recursively to show that the cascade connection of any number of multiport elements in $\mathcal{R}^{2\times 2}$ also belongs to $\mathcal{R}^{2\times 2}$.

We conclude the proof by showing that the scattering matrix elements for lumped circuit blocks and transmission-line structures belong to $\mathcal{R}$. The case of lumped circuits is trivial, since their responses are purely rational. Conversely, the case of transmission-lines, including the lossy and frequency-dependent cases, requires some care and some approximation. We consider in the following a scalar transmission line of length $\mathcal{L}$ with frequency dependent per-unit-length parameters $R(s), L(s), G(s)$, and $C(s)$. We define the propagation factor and characteristic admittance, respectively, as

$$\begin{aligned}
\Gamma(s) &= \sqrt{(R(s) + sL(s))(G(s) + sC(s))} \\
Y_c(s) &= \sqrt{\frac{G(s) + sC(s)}{R(s) + sL(s).}}
\end{aligned}$$

A straightforward calculation leads to the following expressions for the scattering matrix elements:

$$\begin{aligned}
S_{11} = S_{22} &= \frac{-\alpha_+\alpha_-(1-Q^2)}{\alpha_+^2 - Q^2\alpha_-^2} \\
S_{12} = S_{21} &= \frac{Q\left(\alpha_+^2 - \alpha_-^2\right)}{\alpha_+^2 - Q^2\alpha_-^2}
\end{aligned} \tag{30}$$

where

$$\alpha_\pm(s) = Y_c(s) \pm Y_R, \quad Q(s) = e^{-\mathcal{L}\Gamma(s)}$$

with Y_R representing the port reference admittance. Following the well-known Method of Characteristics approach [14], [17], we extract the propagation delay T from the propagation operator

$$Q(s) = e^{-sT}P(s)$$

where $P(s)$ includes no delay and represents mainly frequency-dependent attenuation and dispersion effects. Then, we compute rational approximations for characteristic admittance $\tilde{Y}_c(s) \simeq Y_c(s)$ and delayless propagation operator

$\tilde{P}(s) \simeq P(s)$. Note that the corresponding approximation errors can be reduced below any prescribed threshold due to the universal approximation properties of rational functions [40]. Setting

$$\tilde{\alpha}_{\pm}(s) = \tilde{Y}_c(s) \pm Y_R, \quad \tilde{Q}(s) = e^{-sT}\tilde{P}(s)$$

we can approximate the denominators of (30) with the expansion

$$\begin{aligned}\left(\tilde{\alpha}_+^2 - \tilde{Q}^2\tilde{\alpha}_-^2\right)^{-1} &= \tilde{\alpha}_+^{-2}(1-(\tilde{Q}\tilde{\alpha}_-/\tilde{\alpha}_+)^2)^{-1} \\ &= \tilde{\alpha}_+^{-2}(1-(e^{-sT}\tilde{P}\tilde{\alpha}_-/\tilde{\alpha}_+)^2)^{-1} \\ &= \tilde{\alpha}_+^{-2}\sum_{m=0}^{\infty}(\tilde{P}\tilde{\alpha}_-/\tilde{\alpha}_+)^{2m}e^{-2smT}.\end{aligned}$$

It is easily recognized that this expression belongs to $\mathcal{R}$. This proves that the scattering matrix of frequency-dependent transmission lines belongs to $\mathcal{R}^{2\times 2}$, provided that suitable rational approximations are used for both characteristic admittance and delayless propagation operators.

ACKNOWLEDGMENT

The authors would like to thank C. Schuster, E. Klink, and D. Kaller for sharing the data they used in some of the numerical examples.

REFERENCES

[1] C. K. Sanathanan and J. Koerner, "Transfer function synthesis as a ratio of two complex polynomials," *IEEE Trans. Autom. Control*, vol. 8, no. 1, pp. 56–58, Jan. 1963.

[2] B. Gustavsen and A. Semlyen, "Rational approximation of frequency responses by vector fitting," *IEEE Trans. Power Del.*, vol. 14, no. 3, pp. 1052–1061, Jul. 1999.

[3] B. Gustavsen, "Computer code for rational approximation of frequency dependent admittance matrices," *IEEE Trans. Power Del.*, vol. 17, no. 4, pp. 1093–1098, Oct. 2002.

[4] B. Gustavsen and A. Semlyen, "A robust approach for system identification in the frequency domain," *IEEE Trans. Power Del.*, vol. 19, no. 3, pp. 1167–1173, Jul. 2004.

[5] D. Deschrijver and T. Dhaene, "Rational modeling of spectral data using orthonormal vector fitting," in *Proc. 9th IEEE Workshop Signal Propagat. Interconnects*, Garmisch-Partenkirchen, Germany, May 10–13, 2005, pp. 111–114.

[6] D. Deschrijver, B. Haegeman, and T. Dhaene, "Orthonormal vector fitting: A robust macromodeling tool for rational approximation of frequency domain responses," *IEEE Trans. Adv. Packag.*, vol. 30, no. 2, pp. 216–225, May 2007.

[7] S. Grivet-Talocia and M. Bandinu, "Improving the convergence of vector fitting in presence of noise," *IEEE Trans. Electromagn. Compatibil.*, vol. 48, no. 1, pp. 104–120, Feb. 2006.

[8] S. Grivet-Talocia, "Package macromodeling via time-domain vector fitting," *IEEE Microwave Wireless Compon. Lett.*, vol. 13, no. 11, pp. 472–474, Nov. 2003.

[9] *VectFit2*, [Online]. Available: http://www.energy.sintef.no/produkt/VECTFIT/index.asp

[10] *IdEM 2.4*, [Online]. Available: http://www.emc.polito.it

[11] R. Mandrekar and M. Swaminathan, "Causality enforcement in transient simulation of passive networks through delay extraction," in *Proc. 9th IEEE Workshop Signal Propagat. Interconnects*, 2005, pp. 25–28.

[12] F. H. Branin, Jr., "Transient analysis of lossless transmission lines," *Proc. IEEE*, vol. 55, no. 11, pp. 2012–2013, Nov. 1967.

[13] A. J. Gruodis and C. S. Chang, "Coupled lossy transmission line characterization and simulation," *IBM J. Res. Develop.*, vol. 25, pp. 25–41, Jan. 1981.

[14] F. Y. Chang, "The generalized method of characteristics for waveform relaxation analysis of lossy coupled transmission lines," *IEEE Trans. Microwave Theory Tech.*, vol. 37, no. 12, pp. 2028–2038, Dec. 1989.

[15] S. Lin and E. S. Kuh, "Transient simulation of lossy interconnects based on the recursive convolution formulation," *IEEE Trans. Circuits Syst. I*, vol. 39, no. 11, pp. 879–892, Nov. 1992.

[16] D. B. Kuznetsov and J. E. Schutt-Ainé, "Optimal transient simulation of transmission lines," *IEEE Trans. Circuits Syst. I*, vol. 43, no. 2, pp. 110–121, Feb. 1996.

[17] S. Grivet-Talocia, H. M. Huang, A. E. Ruehli, F. Canavero, and I. M. Elfadel, "Transient analysis of lossy transmission lines: An effective approach based on the method of characteristics," *IEEE Trans. Adv. Packag.*, vol. 27, no. 1, pp. 45–56, Feb. 2004.

[18] N. M. Nakhla, A. Dounavis, R. Achar, and M. S. Nakhla, "DEPACT: Delay extraction-based passive compact transmission-line macromodeling algorithm," *IEEE Trans. Adv. Packag.*, vol. 28, no. 1, pp. 13–23, Feb. 2005.

[19] B. Zhong, T. Hu, D. Fu, S. L. Dvorak, and J. L. Prince, "A study of a hybrid phase-pole macromodel for transient simulation of complex interconnects structures," *IEEE Computer-Aided Design Integr. Circuits Syst.*, vol. 24, no. 8, pp. 1250–1261, Aug. 2005.

[20] A. Charest, D. Saraswat, M. Nakhla, R. Achar, and N. Soveiko, "Compact macromodeling of high-speed circuits via delayed rational functions," *IEEE Microwave Wireless Compon. Lett.*, vol. 17, no. 12, pp. 828–830, Dec. 2007.

[21] S. Grivet-Talocia, "Delay-based macromodels for long interconnects via time-frequency decompositions," in *Proc. IEEE 15th Topical Meeting Electrical Performance Electronic Packag. (EPEP 2006)*, Scottsdale, AZ, Oct. 23–25, 2006, pp. 199–202.

[22] B. Gustavsen, "Time delay identification for transmission line modeling," in *Proc. 8th IEEE Workshop Signal Propagat. Interconnects*, 2004, pp. 103–106.

[23] D. De Zutter and L. Knockaert, "Skin effect modeling based on a differential surface admittance operator," *IEEE Trans. Microwave Theory Tech.*, vol. 53, no. 8, pp. 2526–2538, Aug. 2005.

[24] S. Grivet-Talocia and A. Ubolli, "On relative error minimization in passivity enforcement schemes," in *Proc. 11th IEEE Workshop Signal Propagat. Interconnects*, Ruta di Camogli, Italy, May 13–16, 2007, pp. 75–78.

[25] V. Belevitch, *Classical Network Theory*. San Francisco, CA: Holden-Day, 1968.

[26] M. R. Wohlers, *Lumped and Distributed Passive Networks*. New York: Academic, 1969.

[27] P. Triverio, S. Grivet-Talocia, M. S. Nakhla, F. Canavero, and R. Achar, "Stability, causality, and passivity in electrical interconnect models," *IEEE Trans. Adv. Packag.*, vol. 30, no. 4, pp. 795–808, Nov. 2007.

[28] D. Saraswat, R. Achar, and M. Nakhla, "Global passivity enforcement algorithm for macromodels of interconnect subnetworks characterized by tabulated data," *IEEE Trans. Very Large Scale (VLSI) Syst.*, vol. 13, no. 7, pp. 819–832, Jul. 2005.

[29] C. P. Coelho, J. Phillips, and L. M. Silveira, "A convex programming approach for generating guaranteed passive approximations to tabulated frequency-data," *IEEE Trans. Computed-Aided Design Integrated Circuits Syst.*, vol. 23, no. 2, pp. 293–301, Feb. 2004.

[30] B. Gustavsen and A. Semlyen, "Enforcing passivity for admittance matrices approximated by rational functions," *IEEE Trans. Power Syst.*, vol. 16, no. 1, pp. 97–104, Feb. 2001.

[31] S. Grivet-Talocia, "Passivity enforcement via perturbation of Hamiltonian matrices," *IEEE Trans. Circuits Syst. I*, vol. 51, no. 9, pp. 1755–1769, Sep. 2004.

[32] S. Grivet-Talocia, "An adaptive sampling technique for passivity characterization and enforcement of large interconnect macromodels," *IEEE Trans. Adv. Packag.*, vol. 30, no. 2, pp. 226–237, May 2007.

[33] S. Grivet-Talocia and A. Ubolli, "Passivity enforcement with relative error control," *IEEE Trans. Microwave Theory Tech.*, vol. 55, no. 11, pp. 2374–2383, Nov. 2007.

[34] E. Gad, C. Chen, M. Nakhla, and R. Achar, "Passivity verification in delay-based macromodels of electrical interconnects," *IEEE Trans. Circuits Syst. I*, vol. 52, no. 10, pp. 2173–2187, Oct. 2005.

[35] C. Chen, E. Gad, M. Nakhla, and R. Achar, "Passivity verification in delay-based macromodels of multiconductor electrical interconnects," *IEEE Trans. Adv. Packag.*, vol. 30, no. 2, pp. 246–256, May 2007.

[36] A. Chinea and S. Grivet-Talocia, "A passivity enforcement scheme for delay-based transmission line macromodels," *IEEE Microwave Wireless Compon. Lett.*, vol. 17, no. 8, pp. 562–564, Aug. 2007.

[37] A. Chinea and S. Grivet-Talocia, "Perturbation schemes for passivity enforcement of delay-based transmission line macromodels," *IEEE Trans. Adv. Packag.*, vol. 31, no. 3, pp. 568–578, Aug. 2008.

[38] I. Daubechies, *Ten Lectures on Wavelets*. Philadelphia, PA: SIAM, 1992.

[39] L. Brillouin, *Wave Propagation and Group Velocity*. New York: Academic, 1960.

[40] E. W. Cheney, *Introduction to Approximation Theory*. Providence, RI: Amer. Math. Soc., 1982.

Alessandro Chinea received the Laurea Specialistica (M.Sc.) degree in electronic engineering, in 2006, from the Polytechnic University of Turin, Turin, Italy, where he is currently working toward the Ph.D. degree in the Electromagnetic Compatibility Group.

His research interests concern macromodeling of electrical interconnects for electromagnetic compatibility and signal integrity problems. In particular, he works on algorithms development for passivity check and enforcement of distributed models.

Mr. Chinea received the Optime Award from the Unione Industriale di Torino and he was selected for the IBM EMEA Best Student Recognition Event 2006.

Piero Triverio (S'06) received the Laurea Specialistica degree (M.Sc.) in electronic engineering, in 2005, from the Polytechnic University of Turin, Turin, Italy, where he is currently working toward the Ph.D. degree in the Electromagnetic Compatibility Group.

In 2005 and 2007, he was visiting student with the Computer Aided Design Research Group at Carleton University, Ottawa, ON, Canada. His research interests are in the modeling and simulation of high-speed interconnects.

Mr. Triverio is co-recipient of the 2007 Best Paper Award of the IEEE TRANSACTIONS ON ADVANCED PACKAGING, and the recipient of the INTEL Best Student Paper Award presented at the IEEE 15th Topical Meeting on Electrical Performance of Electronic Packaging (EPEP 2006). He received the Optime Award of the Turin Industrial Association and in 2005 was selected for the IBM EMEA Top Student Recognition Event.

Stefano Grivet-Talocia (M'98–SM'07) received the Laurea and the Ph.D. degrees in electronic engineering from the Polytechnic University of Turin, Turin, Italy.

From 1994 to 1996, he was with the NASA/Goddard Space Flight Center, Greenbelt, MD, where he worked on applications of fractal geometry and wavelet transform to the analysis and processing of geophysical time series. Currently, he is an Associate Professor of Circuit Theory with the Department of Electronics, Polytechnic of Turin. His current research interests are in passive macromodeling of lumped and distributed interconnect structures, modeling and simulation of fields, circuits, and their interaction, wavelets, time-frequency transforms, and their applications. He is author of more than 90 journal and conference papers.

Dr. Grivet-Talocia is co-recipient of the 2007 Best Paper Award of the IEEE TRANSACTIONS ON ADVANCED PACKAGING and received the IBM Shared University Research (SUR) Award in 2007 and 2008. He served as Associate Editor for the IEEE TRANSACTIONS ON ELECTROMAGNETIC COMPATIBILITY from 1999 to 2001.